Implicit-solvent Models for Micellization of Ionic Surfactants

Arben Jusufi, Antti-Pekka Hynninen,
and
Athanassios Z. Panagiotopoulos[*]

Department of Chemical Engineering and

Institute for the Science and Technology of Materials, Princeton University,

Princeton NJ 08544, USA

July 15, 2008

Abstract

We propose a method for parameterization of implicit-solvent models for the simulation of self-assembly of ionic surfactants into micelles. The parameterization is carried out in two steps. The first step involves atomistic Molecular Dynamics simulations of headgroups and counterions with explicit solvent to determine structural properties. An implicit-solvent model of the headgroup/counterion system is obtained by matching structural quantities between explicit-solvent and implicit-solvent systems. In the second step we identify the solvophobic attractions between the tail beads. We determine the solvophobic parameters using Grand Canonical Monte Carlo simulations with histogram reweighting techniques. The matching objective for the

[*]Corresponding author, electronic mail: azp@princeton.edu

1

identification of solvophobic attractions is the critical micelle concentration (cmc). We chose sodium dodecyl sulfate as the reference system. Based on hydrophobic parameters obtained from this particular model we study specific ion effects (lithium and potassium instead of sodium), as well as the effect of cationic headgroups (dodecyltrimethylammonium bromide/chloride). Furthermore, the chain length dependence of micellization properties is investigated for sodium alkyl sulfate, with alkyl lengths between 6 and 14. All cases considered give results in broad agreement to experimental data, confirming transferability of parameters and the generality of the approach.

1 Introduction

Surfactants are amphiphilic molecules that form micelles above a critical micelle concentration (cmc). The driving force for self assembly of surfactants is the interplay of solvophilic interactions of the headgroup and the solvophobicity of the tail. Micellization occurs only above the cmc, since the energetic gain must exceed the entropic costs for the aggregation. The self-assembly process depends on many parameters, such as temperature, salinity, solvent condition, and surfactant architecture.[1–5] Surfactants are used in various applications, from cleaning products[2,3] to nanotechnology,[6,7] and are of particular relevance to biological cell membranes.[1,5]

In the past years many simulation studies have been performed to investigate the self-assembly of ionic surfactants.[8–23] While atomistic and coarse-grained Molecular Dynamics (MD) simulations with explicit water give insight into structural correlations, water penetration and degree of counterion binding of the micelles,[15–21] recent Monte Carlo (MC) studies[23] have also focussed on thermodynamic behavior. Atomistic simulations of surfactants with explicit water involve a significant number of particles, on the order of 5000-50000,[21] or higher. Simulations on time scales that capture the micellization process can only be achieved by large scale computational effort,

because of the presence of a large number of water molecules and the inherently long micellization time scales ($\sim \mu$s and above).[24]

Coarse-grained surfactant and water models are computationally faster than detailed atomistic models, but still involve a significant number of water molecules.[25–30] In contrast, implicit water models with coarse-grained surfactants dramatically improve the computational efficiency of determining thermodynamic and conformational properties, such as the shape and size distribution. As we will show below, the computational benefit of an implicit model compared to a fully atomistic one is about two orders of magnitude saving in CPU (Central Processing Unit) time. Within the implicit-solvent models one should distinguish between continuum models[31–36] and lattice models.[23,37–46] MD simulations of continuum models have been used to capture mainly structural micellar properties for specific surfactants, such as DPC and decyltrimethylammonium chloride.[33–35] Recently, a lattice-based MC simulation study of NaDS has shown to reproduce thermodynamic quantities, such as the cmc and its temperature dependence above room temperature.[23] However, the absolute cmc values determined in Ref. 23 deviate from experimental results by factors of 3-5. This method also does not capture subtle effects caused by specific interaction among the particles on short length scales, because of the coarse lattice model used.

In this work, we develop an off-lattice implicit-solvent model of ionic surfactants with explicit counterions as a model system that fulfills the conflicting requirements of modest computational cost, the prediction of thermodynamic and structural micellar properties, and the incorporation of specific ion interactions. Specific ion interaction effects are not captured by models that represent the solvent as an overall homogeneous dielectric continuum. In recent work,[47] activity coefficients of aqueous salt solutions were well reproduced by an implicit solvent model. In the same spirit we develop here a headgroup ion model, accounting for specific ion effects for both headgroups and counterions. As an example we choose Sodium Dodecyl Sulfate (NaDS)

in water due to the existence of comprehensive experimental studies for this surfactant.[48–64] NaDS serves as a model system for many computational studies regarding the aggregation process and the structural properties of micellar solutions.[10,14,16–21,23] The methodology for the development of an implicit-solvent model of NaDS presented here is transferrable to other surfactant types. Implicit-water models for biologically relevant amphiphilic molecules, like lipids, could be developed using this approach. The model has been kept as simple as possible in order to facilitate application of the methodology to other surfactant types.

This paper is organized as follows. We outline our proposed methodology for development of implicit-solvent models for ionic surfactants in section 2. The methodology consists of atomistic Molecular Dynamics (MD) simulations of headgroups and counterions in explicit water to obtain ion correlations. These ion correlations are then matched by canonical Monte Carlo simulations of headgroups and counterions without explicit water. Matching is achieved by adjusting the parameters of the effective headgroup-ion interactions. Hydrophobic interactions, assigned to the surfactant tail, are obtained from Grand-Canonical Monte Carlo (GCMC) simulations, by computing the equation of state of the surfactant solution and using it to locate the cmc. Hydrophobic parameters are found by matching the computed cmc and micellar aggregation numbers to experimental data. This methodology is applied to NaDS in section 3. Once we have found a convenient parameterization for NaDS we transfer the model to other surfactant systems in order to test its predictive power. In particular we modify the counterions (replacing Li^+ or K^+ for Na^+) (section 4.1) and the headgroup, replacing the anionic sulfate by the cationic trimethylammonium headgroup with Cl^- and Br^- counterions (section 4.2). A further test of the model is the tail length dependence. We study the cmc and aggregation number with respect to the number of tail beads, in the range from 6 to 14 hydrocarbon segments in section 4.3. Finally, in section 5, we discuss the results and give a brief out-

look regarding its potential use for similar amphiphilic systems and possible applications to salt effects on micellization.

2   Simulation Methods

Our proposed simulation methodology for the development of an implicit-solvent model for ionic surfactants consists of two steps:

1. Identification of the solvophilic effect in the implicit-solvent model. We consider the case where the headgroup is the solvophilic segment of the surfactant. This step involves coarse-graining of the ionic headgroups and parameterization of the interaction potential of the implicit-solvent model of the ions (headgroups and counterions). Due to the lack of solvent molecules in the implicit-solvent model, the atomistic details of the headgroups can be omitted and the headgroup molecule is replaced by a spherical particle. The interaction among these headgroups and the counterions is not a potential of mean force but rather consists of a combination of dispersion-, hydration- and Coulomb forces. The parameterization of these forces is found by matching the pair correlation function $g(r)$ from implicit-solvent simulations with that from explicit-solvent simulations. A similar method has been applied previously[47] to develop an implicit-solvent model of aqueous salt solutions.

2. Identification of the solvophobic effect in the implicit-solvent model. The solvophobic effect is modeled by an effective attraction between the tail beads of different surfactants. The strength of the effective attraction is determined so that the cmc obtained from the equation of state matches experimental data. The equation of state is computed from GCMC simulations.

This methodology is general and can be applied to various ionic surfactant types in different solvents. We chose to develop an implicit-solvent model for

aqueous NaDS solution. Exchanging the counterion type (from Na^+ to Li^+ or K^+), or the headgroup type, affects only the hydrophilic part. Hence, for the corresponding systems, only the first step of the methodology needs to be repeated in order to identify the hydrophilic interaction (and the headgroup/counterion interactions). We anticipated that the hydrophobic effect is not affected by those particular changes and the tail parameters from the NaDS model could be used unmodified. In contrast, if one changes the chemical structure of the tail beads the second step of the above methodology needs to be repeated. Finally, changing the solvent requires a complete parameterization.

We now describe the details of the methodology that was applied to NaDS in water. The first step is illustrated in Fig. 1, showing snapshots of explicit and implicit water simulations of headgroups (here $CH_3SO_4^-$) and counterions (here Na^+). The explicit-water simulations were carried out using the MD package GROMACS 3.3[65–67] in the NVT-ensemble (constant particle number N, volume V and temperature T). The system consisted of 10 headgroups ($CH_3SO_4^-$) and 10 counterions (Na^+) with 2130 SPC water molecules in a cubic box of 4nm edge length with periodic boundary conditions. This system size corresponds to a water density of 994.7kg/m^3 and an ionic strength of 0.26mol/l. We fixed the temperature at $T = 298K$ by coupling the system to a Berendsen thermostat with a relaxation time of 0.1ps.[68] Due to their different degrees of freedom the temperatures of ions and solvent were controlled independently in order to facilitate equilibration. The bond lengths of the water molecules were constrained by the SETTLE algorithm.[69] The Particle-Mesh Ewald (PME) method was used for the computation of the Coulomb interaction with grid spacing of 0.12nm. The Coulomb and Lennard-Jones (LJ) cut-off distance was set to 0.9nm. Using a time step of 2fs, we equilibrated the system for 1.5ns and produced data during further 8.5ns. The implicit water simulations were performed using canonical Monte Carlo (MC) simulations with the same box size. Out of the total 10^7 MC steps, 10^6 were

used for equilibration and $9 \cdot 10^6$ for the calculation of the pair correlation functions.
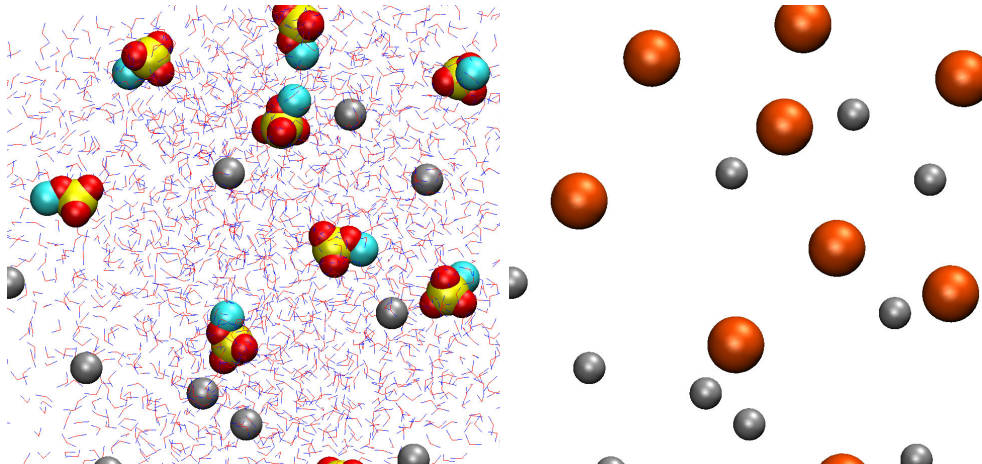

Figure 1: (color online) Snapshots of headgroup segments and counterions (small single spheres). The left picture shows the atomistic case with explicit water (sticks). Note that for this system the atomistic details of the headgroups are taken into account. The right picture shows a snapshot of an implicit-water system with coarse-grained headgroup particles (big spheres) and counterions (small spheres).

In identifying the hydrophobic attraction in the second step we used the GCMC technique in which the volume V, temperature T, and chemical potential μ are kept constant. Unless explicitly specified the cubic box edge length was set to 4.6nm with periodic boundary conditions, and the temperature was fixed at 298K. The surfactant consists of a full tail with the coarse-grained headgroup. Counterions ensuring charge neutrality were added at random positions. There is no explicit water and no added salt. Insertion/deletion moves of surfactant ions are accompanied by insertion/deletion moves of the counterions in order to preserve charge neutrality. Usually 10^7 steps re used for equilibration purposes and further $4 \cdot 10^7$ steps for production. For some cases we extended the equilibration to $4 \cdot 10^7$ steps, depending

on the relaxation behavior observed. We carried out a mix of various MC moves: 10% regrowing of the chains, 35% chain displacements and rotations, 10% counterion displacements, and the remaining 45% insertion/deletion attempts. Configurational-bias was used for the chain regrowth and insertion/deletion moves of the chains.[70] In all MC simulations (canonical MC and GCMC), electrostatics were treated with the Ewald method using 518 Fourier-space vectors and a real-space cutoff of 2.29nm.

The GCMC method allows for the determination of the cmc for given interactions.[23] We performed a series of GCMC calculations at different chemical potentials μ at given temperature for an assumed value of the tail-tail attraction. We started with a small value of μ that usually results in free chain configurations. With increasing μ the density increases as well, until the cmc is reached. By further increase of μ stable micelles are formed. At the same time, we collected histograms of sampled chain numbers and energies of the system at each chemical potential run. With the histogram reweighting technique histograms of several runs can be combined to determine the equation of state.[71] The inflection point in the pressure-density $p(\rho)$-curve yields the cmc.[23] If necessary, the attraction between the tails was tuned, and the whole procedure was repeated until a good match of the model cmc and of experimental results was reached. Hysteresis effects at the target temperature (298K) were addressed with the histogram reweighting technique. Histograms obtained from simulations at higher temperatures (330-360K) without hysteresis effects are combined with histograms obtained at the target temperature.[72,73]

A technical point of interest is the computational efficiency of an implicit solvent model simulation when compared to a corresponding atomistic simulation with explicit solvent molecules. We performed atomistic NVT simulation of 55 NaDS surfactants solvated with 2491 SPC water molecules in a box of edge length 4.6nm. This corresponds to an overall solution density of around 1kg/l. The force field parameters for the surfactants were taken from

Ref. 21. A simulation of 500 000 MD steps (1ns) takes around 10 CPU hours with the GROMACS 3.3 MD package[65–67] on a single processor machine with 2.44GHz. Equilibrium and proper sampling of the system would require at least 200ns[21] corresponding to around 100CPU days. We achieve a similar computation with our implicit solvent model within one day. This corresponds to two orders of magnitude of saving in CPU time and demonstrates the computational benefit in using an implicit-solvent model.

3 Parameterization of implicit NaDS model

Our aim is to obtain a model that matched experimental results for the cmc and the aggregation number for NaDS, using the steps outlined in the previous section.

3.1 The ion interactions

In the implicit solvent simulations we used effective ion interactions for the ions that take hydration layering into account and a distance dependent dielectric permittivity $\epsilon_D(r)$ that amplifies electrostatic interactions at short ion separations, i.e. at contact separations within the hydration layers of the ions. Activity coefficients and structural properties are well reproduced through the use of these effective ion potentials.[47]

We start with the description of an effective interaction potential between the counterions. Due to their repulsive behavior and their minor influence on the micellar properties, we use the primitive model approach: the Coulomb repulsion is amended by the Weeks-Chandler-Anderson (WCA) potential.[74] The Coulomb potential includes a dielectric constant of water ($\epsilon_s = 78$), the remaining free parameters of the WCA-potential are the counterion diameter σ and the prefactor ε, which we assume to be around $\varepsilon = 1kT$. The counterion diameter σ is obtained by matching the radial distribution function $g(r)$ between the Na$^+$ ions from implicit water canonical MC simulations with

that from explicit water MD simulations. For the headgroup atoms, force field parameters are taken from the NaDS model in Refs. 10, 21. For the counterions, the atomistic parameters are obtained from the parameterization of the Huggins-Mayer potential, as was demonstrated by Koneshan et al.[47,75,76]

In the explicit water system $g(r)$ possesses two peaks due to hydration shells. We neglect this complex behavior in the potential ansatz of the counterions within the implicit approach and use a monotonic repulsion between them. A best fit is achieved by using an effective counterion size of $\sigma = 0.31$nm, see inset of Fig. 2.

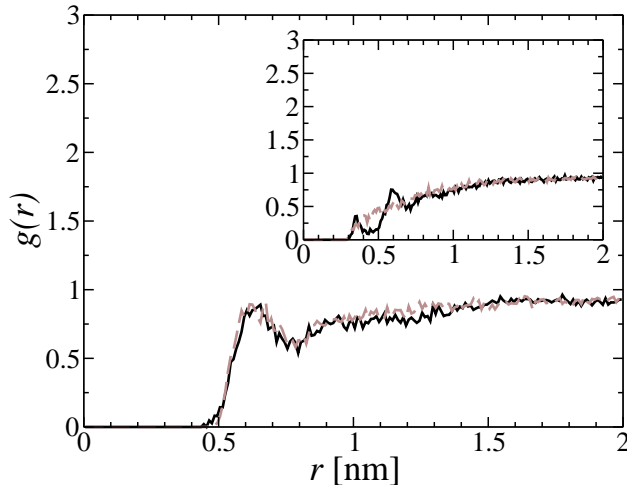Figure 2: (color online) Pair correlation function $g(r)$ among headgroups ($CH_3SO_4^-$) and among Na^+ counterions (inset). Compared are $g(r)$'s from atomistic simulations including explicit water (solid lines) and $g(r)$'s from coarse-grained headgroup-ion simulations with implicit water (dashed lines). For the headgroup the interaction potentials are given in Eqs. (1) - (2) with the parameter values shown in Table I. The counterion repulsion consists of a WCA potential and the Coulomb interaction.

In the same figure the headgroup-headgroup $g(r)$ is shown as well. In the explicit water system, the headgroup-headgroup $g(r)$ has a minimum at

group	σ [nm], ε [kJ mol^{-1}]	H [kJ nm mol^{-1}], r_{mh}, σ_h [nm]	r_{me} [nm]
HG$^-$-HG$^-$	0.543, 1.239	0.076, 0.780, 0.047	
Na$^+$-Na$^+$	0.306, 2.478		
HG$^-$-Na$^+$	0.536, 0.124	0.379, 0.444, 0.034	0.421
Li$^+$-Li$^+$	0.416, 2.478		
HG$^-$-Li$^+$	0.528, 0.124	0.379, 0.3366, 0.007	0.367
K$^+$-K$^+$	0.375, 2.478		
HG$^-$-K$^+$	0.597, 0.124	0.379, 0.390, 0.018	0.444

Table I: Intermolecular potential parameters of headgroup ions (coarse-grained $CH_3SO_4^-$) denoted as 'HG' and counterions for the implicit water simulations. The values corresponds to the best fitting on explicit water results using the atomistic force field parameters for Na$^+$ of Koneshan et al.[77] For Li$^+$ and K$^+$ the fitting was on atomistic results on the basis of the cation force field of Åqvist.[78] The columns show the parameter values of the LJ (U_{LJ}) and hydration potential U_{hydr}. In the last column the values of the inflection point of the dielectric permittivity $\varepsilon_D(r)$ is given, as used in the Coulomb correction term $U_{\text{qq,corr}}$, eq. (4).

around 0.77nm due to hydration. In contrast to the counterion-counterion case, we attempted to reproduce this behavior also in the implicit simulations since the headgroups are in close contact when micelles are formed. For this, we need to modify the interaction potential in the implicit model. The total potential between headgroup ions is:

$$U(r) = U_{\text{LJ}}(r) + U_{\text{qq}}(r) + U_{\text{hydr}}(r). \tag{1}$$

The first term is the LJ potential and the second term is the Coulomb interaction with a dielectric constant $\epsilon_s = 78$. The third term accounts for the repulsive barrier due to a hydration shell modeled by a repulsive Gaussian function:

$$U_{\text{hydr}} = \frac{H}{\sigma_h \sqrt{2\pi}} \exp\left[-\frac{(r - r_{mh})^2}{2\sigma_h^2}\right], \tag{2}$$

with a peak height $H/(\sigma_h\sqrt{2\pi})$, mean r_{mh}, and a standard deviation σ_h.

In Table I the non-bonded parameters for the implicit-water headgroup-ion simulations are summarized. Note that the headgroup ion, the sulfate group, has been coarse-grained, i.e. it is represented by a spherical particle. Since there is no explicit water, the partial charges on the headgroup atoms are of minor relevance. The six partially charged sulfate group atoms $(CH_3SO_4^-)$ are replaced by one charged headgroup particle of valency -1.

The interaction between the headgroups and counterions requires a further contribution. Since the ions attract each other, we also must account for an additional Coulomb correction term due to distance dependence of the dielectric permittivity. This is important at separations smaller than the hydration shell, i.e. close to the hard core contact distance between the ions. As for the implicit-water salt model described in Ref. 47 the total potential between a headgroup ion and a counterion comprises four terms:

$$U_{+-}(r) = U_{LJ}(r) + U_{qq}(r) + U_{hydr}(r) + U_{qq,corr}(r) \tag{3}$$

In comparison to Eq. (1) there is one additional term. The electrostatic energy $U_{qq}(r)$ using a water bulk dielectric constant of $\epsilon_s = 78$ at room temperature needs to be corrected due to the short-range nature of the dielectric permittivity $\epsilon_D(r)$

$$U_{qq,corr}(r) = \frac{1}{4\pi\epsilon_0} \frac{q_i q_j}{\epsilon_s r} \left(\frac{\epsilon_s}{\epsilon_D(r)} - 1 \right), \tag{4}$$

where q_i are the charges of ion i. The dielectric permittivity correction $\epsilon_D(r)$ is proposed to be of the form

$$\epsilon_D(r) = \frac{5.2 + \epsilon_s}{2} + \frac{\epsilon_s - 5.2}{2} \tanh\left(\frac{r - r_{me}}{\sigma_h} \right), \tag{5}$$

where the factor of 5.2 is the limiting permittivity in the vicinity of the ion due to dielectric saturation.[79] This behavior arises from a model for ϵ_D as a function of the electric field in a solvent. The free parameter r_{me} is the

inflection point of the curve, as in Ref. 47. Note that we use for the slope-defining curve the standard deviation σ_h of the hydration potential U_{hydr}. The resulting pair correlation function $g(r)$ is compared to the one obtained from explicit water MD simulations. Results are plotted in Fig. 3. We get
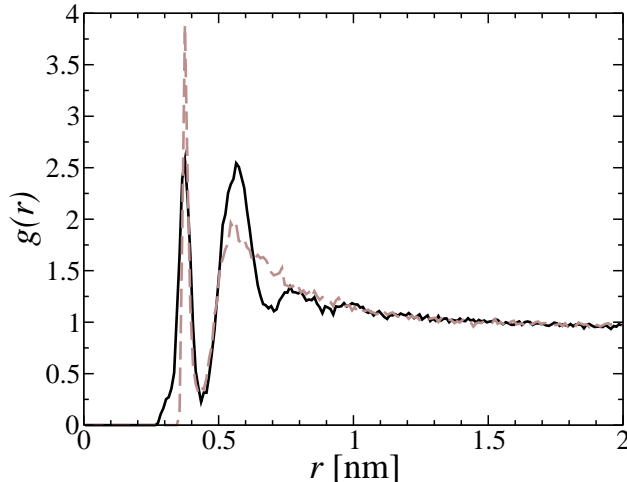

Figure 3: (color online) Pair correlation function $g(r)$ between headgroups and Na^+ counterions, where r is the separation between the centers of mass of the ions, from atomistic simulations including explicit water (solid line) and coarse-grained headgroup-ion simulations with implicit water (dashed line). The areas of the first peaks from the two models are matched.

reasonable agreement between the implicit water results and the explicit water results regarding the essential structure, which would not be possible with a primitive ion model. The double peak is due to hydration layers. In order to ensure that the counterion binding is correctly reproduced, the area of the first peak, rather than its height, has been matched. The first peak is very narrow in the implicit case in comparison to the atomistic one due to the lack of explicit water that causes broader distributions in real systems. As was shown in Ref. 47 for aqueous solutions of alkali metal chloride, the double peak structure has an impact on thermodynamic properties such as the activity coefficient.

One issue in the development of the effective ion interaction lies in the reliability of atomistic reference results. In atomistic studies of NaDS micellization there are different degrees of counterion binding reported, in particular regarding first shell binding.[17–21] The deviations stem from different force field models employed in the atomistic simulations. In our explicit water Na-headgroup studies we used for the Na^+ force field parameters by Koneshan et al.[75,76] We checked the consistency of the atomistic simulations by calculating the $g(r)$ using the force fields by Åqvist[78] and Dang.[80] A comparison of the $g(r)$s did not show any significant difference and had no effects on the micellization behavior.

3.2 The tail group attractions

The bonded properties of the tail of the dodecyl sulfate (DS) surfactant are modeled in a way similar to that of many united atom models, such as OPLS[81] and TraPPE.[82] Coarse-graining of the tail beads was not carried out in order to avoid introducing additional parameters for the bonded interaction potentials. We chose to keep the atomistic settings for the bonded potentials since they are not affected by the presence of water.

The bond length was fixed at $b_0 = 0.153$ nm and harmonic angle and dihedral potentials were employed where the parameters were set equal to the atomistic values.[10] The non-bonded potentials of the tail groups are of LJ type. The LJ diameter was chosen to be $\sigma = 0.395$ nm, appropriate for methylene in the OPLS force field. The exact value is unknown in implicit water simulations. The LJ prefactor ε accounts for the hydrophobic attraction and remains as a fit parameter, that was tuned to match the cmc.

We estimated its value by making the following simple assumption for NaDS. The Laplace pressure of a spherical cavity in a liquid is given by $\Delta p = 2\gamma/R$, where $\gamma = 0.051$N/m is the interfacial tension of water/oil,[83] and R the radius of the cavity. In order to generate such a cavity of size R, it is necessary to employ work of $W = 8\pi\gamma \int_0^R r\,dr = 4\pi\gamma R^2$. This is identical

to the solvation energy for solutes with sizes more than 1nm.[84] Taking an experimental value of $R = 1.84$ nm we obtain $W = 530kT$.[1] This work is needed to create a cavity of size R and is of the same order of magnitude as the energy for dodecylphosphocholine (DPC) micelle formation.[35] It corresponds to the energy gain of the tail beads inside the aggregate due to hydrophobic attraction. Taking an aggregation number of $M = 74$ and a coordination number z of four chains around each tail within the micelle, the energy per chain contact is $w = W/(zM) \approx 1.8kT$.[1] Other experimental values from Berr and Jones ($R \approx 2.27$nm and $M \approx 54$),[53] yield $w = 3.7kT$ per chain. These values comprise a relatively broad range, and should be considered as crude estimates only. Accurate thermodynamic models are given for example in Refs. 5 and 85. Nevertheless, as we will see, our simple model gives reasonable starting values for ε.

The next question is how to distribute this energy along the beads. The common way is to distribute the energy equally along each tail bead. For DS the value range for each tail bead would then be $\varepsilon = w/12 = (0.15 \ldots 0.31)kT$, taking the above work for the cavity formation.

However, as we will show in the next section, an equal distribution of w along the tail molecules does not give the right shape and aggregation number of the micelles. It is important to recall the hydrophobic mechanism of the micellization process. At low surfactant concentration the solution consists of free chains. In an implicit water solvent it is an ideal gas of NaDS. In reality, however, the chains are covered by water molecules. Above the cmc, the molecules start aggregating, driven by rearrangements of the water molecules around the surfactants.[84] The solvation energy for cluster formation is $\sim R^2\gamma$. Water forces the surfactants to build micelles in order to avoid contact with the hydrophobic tails and to maximize the contact with the hydrophilic headgroups. In this way the headgroups are placed on the aggregate surface while the tail beads are buried inside, yielding characteristic morphologies, such as spherical micelles. In an implicit water model, however, there is no

particular need for the aggregates to form such morphologies. Preliminary simulations using an equal attractive strength between the tail beads did not result in spherical micelles. The observed aggregates consisted of around 25 surfactants, a value that is too low. One can increase the aggregation number by increasing ε. In this case, however, the cmc drops, so it is impossible to simultaneously match the cmc and the aggregation number. Although it is common in implicit continuum polymer models to assign the same short range effective attraction to all monomers[86] the application of the same idea on implicit models of surfactants does not produce realistic micellar aggregates.

An alternative approach for an implicit solvent model of surfactants has been proposed by Lazaridis et al.[35] They applied the EEF1 solvation model originally developed for protein simulations[87] on an implicit-water model for DPC. Within this concept the atoms possess solvation barriers of a Gaussian form, in addition to the van-der-Waals interaction. The hydration barrier in Eq. (2) has been introduced in the same spirit. The difference is that all atoms possess a solvation energy, except the ones deeply buried within the molecule. The method is very successful, but requires also adjustment of the solvation free energy of some atoms in order to yield aggregation numbers close to experimental values.[35] An alternative parameterization of an implicit-water model of ionic surfactants and alkanes in water has been proposed by Shinto et al.[33, 34, 36] Their model development is based on the potential of mean-force fitting of surfactant segments and the consideration of free energy changes upon transferring charged headgroups across the oil/water interface. This model describes the structural properties of oil droplets in water and micelles comprised of decyltrimethylammonium alkyl chloride. In particular, the structural correlation of the tail segments in the interior of the micelles agree well with atomistic and experimental results.

In this work we follow a different approach for modeling the hydrophobic effects. Instead of distributing the energy per chain over all beads, we concentrate the hydrophobic attraction on the terminal tail groups in order

16

to favor formation of spherical micelles. All other tail beads still possess a LJ interaction, but with parameters corresponding to the van-der-Waals attraction interaction of the OPLS force field, where $\varepsilon = 0.49$kJ/mol and $\sigma = 0.395$nm.[81] The same OPLS force field is used between the terminal tail bead of one surfactant and the non-terminal tail beads of other surfactants. The tail - headgroup and the tail - counterion interaction is modeled by a purely repulsive LJ potential (WCA potential) using arithmetic averages for the corresponding LJ-diameters of the ions (see Table I) and tail segments ($\sigma = 0.395$nm). The LJ energy scale for those interactions is set to $1kT$=2.45kJ/mol. The advantage of this method is its simple implementation in common MD or MC codes. In the next section we demonstrate that this approach achieves values for the cmc and aggregation number close to the experimental values.

3.3 Critical Micelle Concentration and Aggregation Number of NaDS

As stated in Section 3.2, the strength of the terminal tail bead attraction ε_t is adjusted by matching the GCMC results of the cmc on the experimental value for NaDS micelle formation. Figure 4 shows the equation of state $p(\rho)$ for $\varepsilon_t = 9.75\varepsilon = 1.95kT$ (4.8 kJ/mol) that clearly exhibits two linear regimes. The cmc is defined as the inflection point of the $p(\rho)$ curve and we obtain 9.3 ± 0.3mM. This is in agreement with experimental measurements that report values between 7.7mM[58] and 9.3mM[61] at around 298K, depending on the methods. The corresponding energy for micelle formation lies in the range of the estimated solvation energy per surfactant 1.8-3.7kT, see Sec. 3.2.

A typical micellar configuration is shown in Fig. 5. The micelle consists of 61 chains and possess a roughly spherical shape. From the GCMC simulations we determined the distribution of the aggregate size. We define the aggregate with a simple cut-off criterion: two surfactants belong to the same
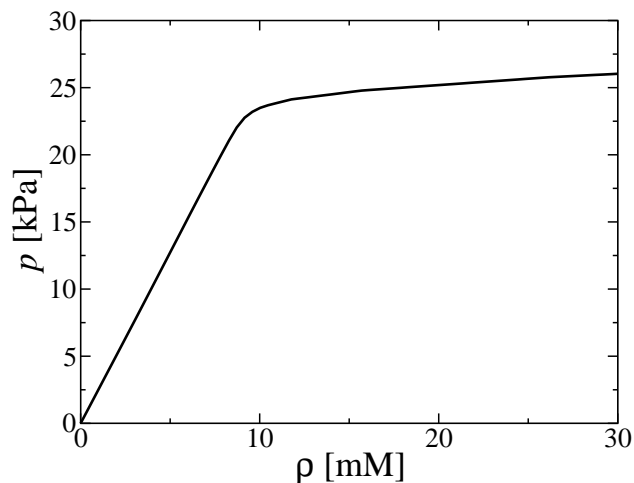
Figure 4: Pressure p versus surfactant density ρ of NaDS-surfactant. The crossover in the curve corresponds to the onset of micellization. The inflection point of the curve defines the cmc.

micelle if the center of mass of one tail is separated by less than 0.4nm from that of another tail. This cut-off value was tested to give the right aggregation number. At very high densities this criterion can become problematic, and more sophisticated criteria should be used.[21] Figure 6 shows the normalized probability distribution of the aggregation number M for three runs, each starting at different initial micellar states of aggregation number M_0, but at the same chemical potential. We used chemical potential value close to the cmc. Evidently the equilibrated micelles from the different runs end up with the same mean aggregation number of around 57. We note that starting the simulations in the dilute free surfactant state does not lead to micelle formation at the same chemical potential due to strong hysteresis effects at 298K, as mentioned in Section 2. Experimental studies at or close to the cmc report aggregation numbers around 50.[53] Other experimental works report wide distributions in M, ranging from 50[57] up to 64[64] for NaDS. Our results are within the reported range. The distributions are akin to Gaussian distri-
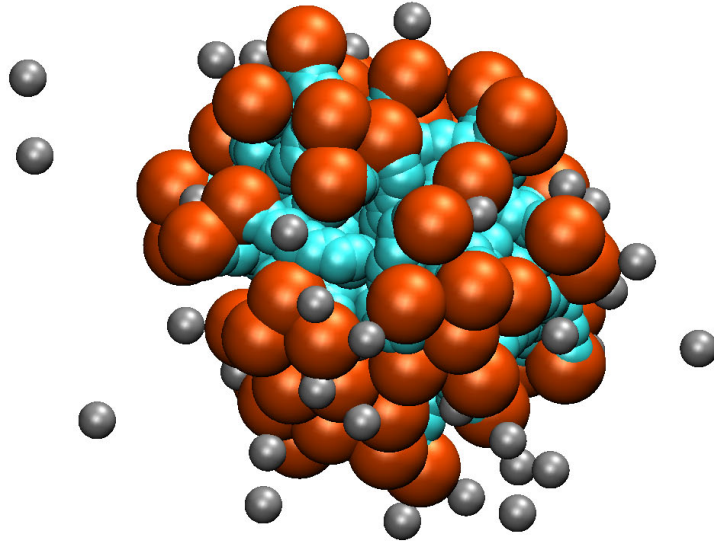
18

Figure 5: (color online) Snapshot of a NaDS micelle with aggregation number $M = 61$. The coarse-grained headgroups (big spheres) are surrounded by counterions (single dark spheres). The tail beads (bonded small spheres) are buried inside the micelle.

butions, in line with experimental observations.[1] The standard deviation of the aggregate size is around 6.

The finite size effects on the cmc and the aggregation number were checked by varying the box size. This is equivalent to varying the overall surfactant concentration. For box lengths 6.1nm and 15.3nm, we obtained cmc values 9.5mM and 7.1mM, respectively. The first value (9.5mM) is within error bars of the original cmc (9.3 ± 0.3)mM. Note that we use the equation of state for the cmc determination, see Fig 4. This is equivalent to the free surfactant calculation, since those are dominantly osmotically active. A cmc drop corresponds therefore to a decrease in the free surfactant concentration, which particularly occurs at large box sizes, as was also reported in Ref. 23.
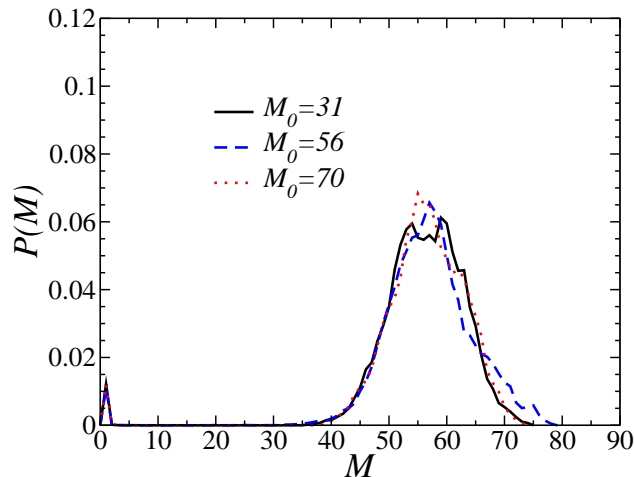
Figure 6: (color online) Normalized probability distribution of the aggregation numbers M for NaDS-surfactants from three runs starting at different states with micelles of aggregation number M_0. The mean aggregation number of all runs is $\langle M \rangle = 57$ with a standard deviation of around 6.

Nevertheless, all values are still close to experimental results (7.7-9.3mM). The aggregation number does hardly change with the increase of the box size. At 6.1nm box length the mean aggregation number remains at 57 and at 15.3nm we obtain an average value of 54. Only the standard deviation increases from 7 at $L = 4.6$nm to 10 at $L = 6.1$nm and $L = 15.3$nm. There is only one micelle in all boxes we considered. We conclude that even with the smallest box sizes we obtain reasonable simulation results for the aggregation number and the cmc.

3.4 Structural properties

We studied the structure of a NaDS micelle at the cmc. From the principal moments of inertia $I_1 \geq I_2 \geq I_3$ of the micelle we obtain information about the shape of the micelle. The ratios $I_1/I_2 = 1.02$ and $I_1/I_3 = 1.24$ indicate a modest ellipsoidal shape with respect to one principal axis. This is in

line with atomistic studies[16,17,19,21] and experimental measurements.[53] The aspect ratio increases with increasing aggregate size, i.e. at higher surfactant concentration.

We analyzed the internal structure of the micelle as well. Figure 7 shows the probability distributions $4\pi r^2 \rho(r)$, with $\rho(r)$ being the radial density distribution of various surfactant segments and counterions with respect to the micelle's center of mass.
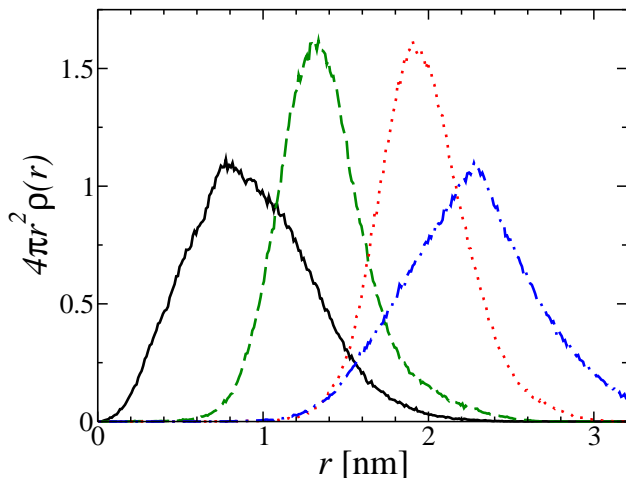

Figure 7: (color online) Normalized probability distribution of terminal tail beads (C12), mid tail segments (C6), headgroups and Na$^+$ counterions as function of the distance r from the center of mass of a micelle with an average aggregate size of 55 NaDS surfactants.

Despite the stronger attraction of the terminal tail beads, their density distribution, and also that of the mid-term beads, is broad, indicating liquid-like disorder in the interior of the micelle. The density of the headgroups peaks further away from the center of the micelle and defines the micellar surface. The counterions are localized close to the micellar surface as well. The distributions are quite similar to these seen from atomistic simulations[18,21] and show also similar characteristics as the implicit-solvent model (ISM-2) study of Decyltrimethylammonium chloride micelles.[34] The average

position of the headgroups with respect to the center of mass of the micelle is (1.96±0.03)nm, and is in excellent agreement with the values obtained from atomistic simulations (1.97nm,[16]1.96nm,[17] 1.99nm,[19] (1.8-2.0)nm[21]). We checked also system size effects and observed almost no change in the profiles of the surfactant segments. Since there is only one micelle in the system with aggregation numbers of around 55 only the counterion probability distribution is different due to a change in the overall counterion concentration. The maximum of the counterion peak, however, remains at the micellar surface, irrespective of the system size.

4   Model transferability

In the previous section an implicit water model for NaDS micelles was developed. The model was adjusted to match the cmc of experimental results. The resulting aggregation number is also within the range of experimentally reported values. In this section we test the sensitivity of the model by exchanging the counterion and headgroup types. We keep the parameter settings of the tail beads as determined for NaDS. Furthermore, we modify the tail length and keep the sulfate headgroup parameters fixed. We check the chain length dependence of the cmc and the aggregation number.

4.1   Specific ion effects

In order to check the model for subtle changes in surfactant properties, we exchanged Na^+ by other alkali metal ions, such as Li^+ and K^+. In our model we need to modify the headgroup-counterion interactions to account for this exchange. The methodology is the same as described in Sec. 3.1.

An exchange of sodium ions by Li^+ and K^+ gives rise to differences in the headgroup-counterion interaction. In the explicit water ion simulations we used the approach of Koneshan et al. using values of Pettitt et al. for the Li^+ and K^+ potential parameters.[75,76] The values are given in Ref. 47. We also

used another parameter set by Åqvist.[78] There are qualitative differences in the $g(r)$ between the two parameter sets. The use of Åqvist parameters give rise to a first counterion binding peak, see Fig. 8. The parameter
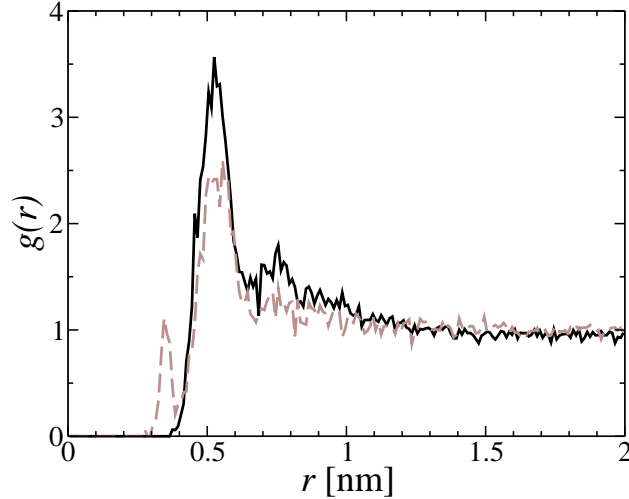

Figure 8: (color online) Li-headgroup $g(r)$ (headgroup: $CH_3SO_4^-$) obtained from explicit water MD simulations using the force field parameter for Li^+ according to the settings given in Ref. 47 (solid line). The dashed curve result if one uses the Åqvist force field.[78]

setting of Ref.47 does not possess a first peak, but a pronounced second ion binding shell at around 0.5nm. We fitted both $g(r)$s shown in Fig. 8 with the ones obtained from implicit water simulations using interaction potentials presented in Sec. 3.1. The implicit model parameters obtained from the fitting of the atomistic Åqvist results are given in Table I. We determined the cmc for LiDS using these Li-headgroup parameters and keeping the tail bead interactions the same as for NaDS. We obtained cmc of 9.1 mM using the fit to the Åqvist force field parameterization and 7 mM using the Li^+-parameterization given in Ref. 47. In comparison to the experimental cmc (ca. 8.9 mM),[50,55,88] the Åqvist force field is a better choice.

In contrast to LiDS, for KDS both Koneshan and Åqvist fit parameters

yield the same cmc. The results of cmc and aggregation number are summarized in Table II and compared to experimental findings. They deviate around 10-20% from each other; the simulation uncertainty is around 5% for the cmc and the standard deviation of the aggregation number is around $\sqrt{M}$, as shown in Fig.6. The experimental trend cmc(KDS) < cmc(NaDS) < cmc(LiDS) could not be reproduced. Instead, the simulations show the opposite trend. The reason for this discrepancy could be due to the atomistic force field used in the parameterization of the headgroup-counterion interactions since, as we showed above for LiDS case, the implicit water simulation results are sensitive to the choice of the headgroup-counterion interaction.

surfactant	cmc [mM]		M	
	sim.	exp.	sim.	exp.
LiDS	9.1	8.7^a, 8.9^b	49	50^b, 54^d
NaDS	9.3	7.7^e, 8.2^a, 8.3^b, 9.3^f	57	50^g, 53^d, 64^h
KDS	10	6.7^f, 7.2^b	55	60^b
DTAB	16.4	14.6^h, 14.9^i	35	49^h, 55^i
DTAC	22.2	17.2^j, 20.3^i, 21.3^k	31	45^i

^{a}Ref. 55, ^{b}Ref. 50, ^{c}Ref. 88, ^{d}Ref. 53, ^{e}Ref. 58, ^{f}Ref. 61, ^{g}Ref. 57, ^{h}Ref. 64, ^{i}Ref. 91, ^{j}Ref. 89, ^{k}Ref. 90

Table II: The cmc and aggregation number for Alkali metal dodecyl sulfates (DS), and dodecyl trimethylammonium halodides. Given are simulation results and experimental data from different studies. The simulation uncertainties are around 5% for the cmc, while the standard deviation for the aggregation number scales with $\sqrt{M}$.

A final remark regarding the hydrophobic energy scale ε_t should be made. The value used was taken for a specific surfactant type, namely NaDS. Influences of the headgroup and counterion type on the hydrophobic interactions are also included in this parameter. However, this contribution is small compared to the hydrophobicity of the hydrocarbon tails. However for subtle effects on the micellization, such as specific ion effects, those contributions could be important. Studies have shown that the interfacial tension of LiDS

is different from that of NaDS.[92] Hence, a further potential error source could be the fact that the hydrophobic energy scale ε_t was taken to be equal to that of NaDS. This could lead to slightly different values of ε_t in the case of LiDS or KDS, which was not taken into account in the present model.

4.2 Variation of headgroup type

The anionic headgroup of NaDS is replaced by a cationic one by keeping the tail unchanged. We chose dodecyl trimethylammonium bromide (DTAB) and the same headgroup with Cl^- ions (DTAC). The headgroup segment consists of $N(CH_3)_4^+$ cation. Since the tail bead is unchanged we only need to parameterize the headgroup and the counterion (Br^-/Cl^-). Using the same procedure as in Section 3.1 we performed explicit water MD simulations of the headgroup and the counterions. The force field parameters of the headgroup are taken from Jorgensen et al.[93] The atomistic parameters of Cl^- are taken from Koneshan et al.[75,76] and that of Br^- from Bhatt et al.[94] The implicit model uses again the same interaction potentials with parameters which need to be determined through a fit of the corresponding $g(r)$s. In both cases, a

group	σ [nm], ε [kJ mol^{-1}]	H [kJ nm mol^{-1}], r_{mh}, σ_h [nm]
HG^+-HG^+	0.788, 0.173	0.084, 1.033, 0.045
Br^--Br^-	0.496, 2.478	
HG^+-Br^-	0.536, 0.124	0.084, 0.699, 0.038
Cl^--Cl^-	0.490, 2.478	
HG^+-Cl^-	0.490, 0.099	0.038, 0.669, 0.038

Table III: Intermolecular potential parameters of headgroup ions (denoted as 'HG') and counterions (Br^-, Cl^-) in the implicit water simulations for the cationic $N(CH_3)_4^+$ system. The columns show the parameter values of the LJ (U_{LJ}) and hydration potential U_{hydr}. A Coulomb correction term $U_{qq,corr}$ is not required due to a lack of a first counterion binding shell.

first counterion binding shell is missing, in contrast to the anionic dodecyl

cases, see Fig. 3. We therefore leave out the Coulomb correction term in the total interaction potential Eq. (3), and use the ansatz (1). A best fit of the atomistic results by implicit calculations is achieved with the parameters given in Table III. With these parameter settings we obtained cmcs of 16.7 mM and 17.6 mM for DTAB and DTAC, respectively. These values are in reasonable agreement with experimental data,[64,89–91] see Table II. Note that the cmcs of both DTAB and DTAC are considerably larger than the cmc of the NaDS. We also note that the micelles formed by DTAB and DTAC are significantly smaller than the micelles formed by NaDS. The aggregation number of DTAB is around 35, smaller than the experimental value of 55.[91] Our model for DTAC gives rise to slightly smaller aggregates, ($M \approx 31$), compared to DTAB, in line with experimental observations, see Table II. The model gives the correct trends by going from the anionic DS to the cationic DTA and yields realistic cmc values. We stress that the parameter settings for the tail have been left unchanged, so those results are pure predictions.

4.3   Variation of chain length

We now investigate the chain length dependence of the cmc and aggregation number of SnS (sodium n-alkane sulfate), i.e. we change the number of tail beads n, but keep the sulfate headgroup and Na$^+$ counterions. According to experiments, the cmc and the aggregation number are significantly affected by the choice of the chain length n. Experiments show that the cmc ranges from 2mM to 420mM, while the aggregation number is between 17 and 80 for tail length between 6 and 14.[64] The complete parameter settings of NaDS are used, i.e., also the value of the hydrophobic energy scale has been kept constant for all chain lengths n. Using GCMC simulations we determined the cmc and the aggregation number for various cases. The simulation results for the cmc are presented together with experimental data[64,95] in Fig. 9. Both the computed cmc and experimental data show an exponential decay with n, according to Traube's rule.[96] The agreement is remarkable since no further
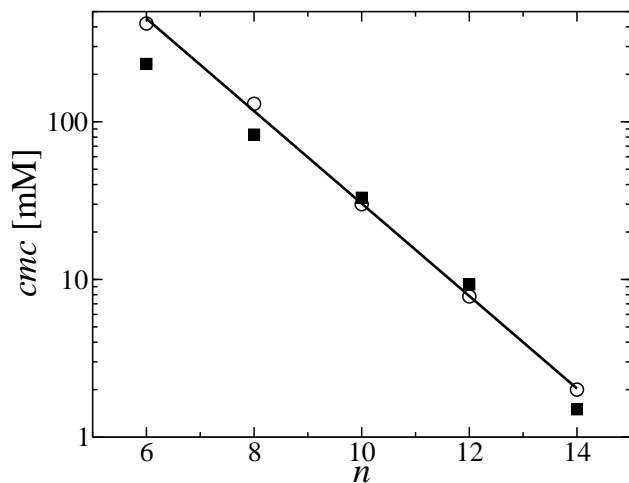
26

Figure 9: cmc for sodium alkane sulfate (SnS) at different chain lengths n. Compared are simulation results (filled squares) with experimental data (open circles).[64,95] The line is an exponential fit to the experimental data. The box size is 4.6nm for $n = 6 - 12$ and 5.4nm for $n = 14$.

adjustments of the model parameters were employed. The aggregation numbers shown in Fig. 10 are also in the range of reported experimental data. The experimental values can be described by a linear fit $M(n)$, that also describes our results up to $n = 12$. For S14S our value is around $M = 100$ values, whereas Nishikido et al. measured a value of $M = 136$.[97] More recent studies, however, report values between 71-89, but at slightly higher temperature (303K).[64,91,95,98] A value of 71 is shown in the plot. One can expect a better agreement with our result if the simulation were carried out at higher temperature, since the aggregate size decreases with increasing temperature.

5   Discussion and Outlook

We developed an approach to obtain implicit-solvent models for ionic surfactants. The development of the model was conducted in two steps. First,
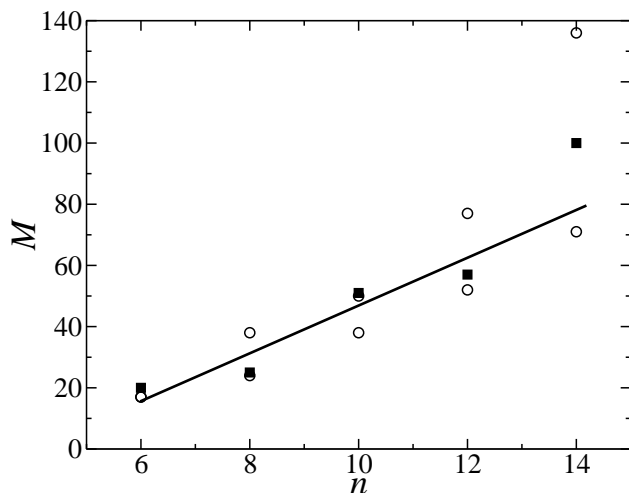
Figure 10: Dependence of aggregation number M with chain length n (number of tail beads). Compared are simulation results (filled squares) with experimental data (open circles).[64,91,95,97,98] A linear dependence (solid line) of the experimental data for $n \leq 12$ is shown as well. The box size is 4.6nm for $n = 6 - 12$ and 5.4nm for $n = 14$.

we identified the solvophilic contribution in an implicit-solvent surfactant model. We performed atomistic Molecular Dynamics simulations of headgroups and counterions in explicit solvent. The radial distribution function between the ions served as a reference for the corresponding canonical Monte Carlo simulations of coarse-grained headgroups and counterions without explicit water. The effective interactions between like-charged counterions is described by the sum of a short ranged purely repulsive LJ potential (WCA potential) and a Coulomb-potential. In contrast, headgroup-headgroup interactions include, in addition to a LJ- and Coulomb potential, a hydration barrier contribution. The cross-interaction contains a further contribution, if a first ion binding shell is observed, as, e.g., in the sodium-sulfate case. This contribution accounts for a short-ranged distance dependent dielectric permittivity that requires a Coulomb-correction.

In a second step, we developed an implicit model for the surfactant tails in

order to quantify the solvophobic contribution of the model. As a demonstration we chose NaDS in aqueous solution. For the development of a tail-tail interaction we took a simple approach. Our aim was to develop an implicit solvent model for NaDS, that is capable in matching both the cmc and the aggregation number to the experimental values. According to our results, using equal strength of attraction ε between all tail beads can reproduce the cmc very well, but did not yield the desired aggregation number. The aggregation number with such models is too small. Conversely, one could achieve reasonable values for the aggregation number by increasing the LJ energy ε further. However, that causes a drop in the cmc, away from realistic values of around 7-8mM. In our approach, this problem was solved by focusing the solvophobic attraction on the terminal tail beads only. We demonstrated that with this approach the cmc and aggregation numbers can be set simultaneously to realistic values. Furthermore, structural properties, such as the probability distributions of surfactant segments agree very well with those obtained from atomistic simulation studies. The key parameter of the present model is the LJ energy of the terminal groups ε_t. whereas the LJ energy of the other tail beads could be set to the ones used in a common atomistic model (OPLS). We note that this hydrophobic energy contains also hydrophobic contributions due to the headgroup and counterion type of NaDS. Those contributions are, however, small compared to the hydrophobic contributions from the hydrocarbon tail beads.

Having obtained a realistic model for micelle formation, we applied the model to cationic surfactants (DTAB, DTAC) and to sodium alkane sulfates (SnS) of different chain lengths. For all these cases, the resulting cmc and aggregation number were in satisfactory agreement with the experiments. We observed that more subtle effects, like specific ion effects, are sensitive to the headgroup-ion interactions that in turn are sensitive to the choice of the atomistic force field and could not be reproduced precisely.

We demonstrated that our implicit solvent model reproduces thermody-

namic and structural properties for all systems considered in this work. A further test of the model would be to study effects of added salt on the micellization process. In fact, first simulation results of NaDS in 0.1M NaCl agree very well with reported experimental values for the cmc. Further studies are in progress and will be published elsewhere. We also plan to extend the methodology to further surfactant systems in other solvents than water and determine the required parameters in order to seek realistic micelle forming conditions. The approach could also be applied on surfactant types of biological relevance, such as lipids.

Acknowledgments

References

(1) Israelachvili, J. N. *Intermolecular and Surface Forces*; Academic Press: Orlando, FL, 1985.

(2) Rosen, M. J. *Surfactants and Interfacial Phenomena, 2nd ed.*; Wiley: New York, NY, 1989.

(3) Tanford, C. *The Hydrophobic Effect: Formation of Micelles and Biological Membranes, 2nd ed.*; Krieger Publishing Co.: Malabar, FL, 1991.

(4) Myers, D. *Surfactant Science and Technology, 2nd ed.*; VCH Publishers: New York, NY, 1992.

(5) Evans, D. F.; Wennerström, H. *The Colloidal Domain: Where Physics, Chemistry, Biology, and Technology Meet*; Wiley-VCH, 2nd ed. 1999.

(6) McGrath, K. M.; Dabbs, D. M.; Yao, N.; Aksay, I. A.; Gruner, S. M. *Science*, **1997**, *277*, 552.

(7) Faul, C. F. J.; Antonietti, M. *Adv. Mater.*, **2003**, *15*, 673.

(8) Jönsson, B.; Edholm, O.; Teleman, O. *J. Chem. Phys.*, **1986**, *85*, 2259.

(9) Watanabe, K.; Ferrario, M.; Klein, M. L. *J. Phys. Chem.*, **1988**, *92*, 819.

(10) Schweighofer, K. J.; Essmann, U.; Berkowitz, M. *J. Phys. Chem. B*, **1997**, *101*, 3793.

(11) Maillet, J. B.; Lachet, V.; Coveney, P. V. *Phys. Chem. Chem. Phys.*, **1999**, *1*, 5277.

(12) Tieleman, D. P.; van der Spoel, D.; Berendsen, H. J. C. *J. Phys. Chem. B*, **2000**, *104*, 6380.

(13) Marrink, S. J.; Tieleman, D. P.; Mark, A. E. *J. Phys. Chem. B*, **2000**, *104*, 12165.

(14) Boek, E. S.; Jusufi, A.; Löwen, H.; Maitland, G. C. *J. Phys.: Condens. Matter* **2002**, *14*, 9413.

(15) Shelley, J.; Watanabe, K.; Klein, M. L. *Int. J. Quantum Chem.*, **1990**, *38*, 103.

(16) MacKerell, A. D. *J. Phys. Chem.*, **1995**, *99*, 1846.

(17) Bruce, C. D.; Berkowitz, M. L.; Perera, L.; Forbes, M. D. E. *J. Phys. Chem. B*, **2002**, *106*, 3788.

(18) Bruce, C. D.; Senapati, S.; Berkowitz, M. L.; Perera, L.; Forbes, M. D. E. *J. Phys. Chem. B*, **2002**, *106*, 10902.

(19) Rakitin, A. R.; Pack, G. R. *J. Phys. Chem. B* **2004**, *108*, 2712.

(20) Yoshii, N.; Okazaki, S. *Chem. Phys. Lett.* **2006**, *426*, 66.

(21) Sammalkorpi, M.; Karttunen, M., Haataja, M. *J. Phys. Chem. B* **2007**, *111*, 11722.

(22) Jorge, M. *Langmuir* **2008**, *24*, 5714.

(23) Cheong, D. W.; Panagiotopoulos, A. Z. *Langmuir* **2006**, *22*, 4076.

(24) Alexandridis, P.; Holzwarth, J. F., Hatton, T. A. *Langmuir* **1993**, *9*, 2045.

(25) Gelbart, W. M.; Ben Shaul, A. *J. Phys. Chem.* **1996**, *100*, 13169.

(26) Goetz, R.; Lipowsky, R.; *J. Chem. Phys.* **1998**, *108*, 7397.

(27) Bandyopadhyay, S.; Klein, M. L.; Martyna, G. J.; Tarek, M. *Mol. Phys.* **1998**, *95*, 377.

(28) Shelley, J. C.; Shelley, M. Y. *Curr. Opin. Colloid Interface Sci.* **2000**, *5*, 101.

(29) Marrink, S. J.; de Vries, A. H., Mark, A. E *J. Phys. Chem. B* **2004**, *108*, 750.

(30) Gao, J.; Ge, W.; Hu, G.; Li, J. *Langmuir* **2005**, *21*, 5223.

(31) Drouffe, J.-M.; Maggs, A. C.; Leibler, S. *Science* **1991**, *254*, 1353.

(32) Bast, T.; Hentschke, R. *J. Mol. Model.* **1996**, *2*, 330.

(33) Shinto, H.; Morisada, S.; Miyahara, M.; Higashitani K. *Langmuir* **2004**, *20*, 2017.

(34) Morisada, S.; Shinto, H.; Higashitani K. *J. Phys. Chem. B* **2005**, *109*, 11762.

(35) Lazaridis, T.; Mallik, B.; Chen, Y. *J. Phys. Chem. B* **2005**, *109*, 15098.

(36) Morisada, S.; Shinto, H.; Higashitani K. *J. Chem. Theory Comput.* **2007**, *3*, 1163.

(37) Haan, S.; Pratt, L. *Chem. Phys. Lett.*, **1981**, *79*, 436.

(38) Larson, R.; Scriven, L.; Davis, H. *J. Chem. Phys.*, **1985**, *83*, 2411.

(39) Care, C. *J. Phys. C: Solid State Phys.*, **1987**, *20*, 689.

(40) Care, C. *J. Chem. Soc., Faraday Trans.*, **1987**, *83*, 2905.

(41) Brindle, D.; Care, C. *J. Chem. Soc., Faraday Trans.*, **1992**, *88*, 2163.

(42) Larson, R. *J. Chem. Phys.*, **1992**, *96*, 7904.

(43) Bernardes, A.; Henriques, V.; Bisch, P. *J. Chem. Phys.*, **1994**, *101*, 645.

(44) Mackie, A. D.; Panagiotopoulos, A. Z.; Szleifer, I. *Langmuir*, **1997**, *13*, 5022.

(45) Nelson, P. H.; Rutledge, G. C.; Hatton, T. A. *J. Chem. Phys.* **1997**, *107*, 10777.

(46) Floriano, M. A.; Caponetti, E.; Panagiotopoulos, A. Z. *Langmuir*, **1999**, *15*, 3143.

(47) Lenart, P. J.; Jusufi, A.; Panagiotopoulos, A. Z. *J. Chem. Phys.* **2007**, *126*, 044509.

(48) Stigter, D.; Mysels, K. J. *J. Phys. Chem.*, **1955**, *59*, 45.

(49) Goddard, E.; Benson, G. *Can. J. Chem.*, **1957**, *35*, 986.

(50) Mukerjee, P.; Mysels, K. J.; Kapauan, P. *J. Phys. Chem.*, **1967**, *71*, 4166.

(51) Haytar, J. P.; Penfold, J. *Colloid Polym. Sci.*, **1983**, *261*, 1022.

(52) Johnson, I.; Olofson, G.; Jönsson, B.; Mishra, B. K.; Puri, P. M. *J. Chem. Soc. Faraday Trans. 1*, **1987**, *83*, 3331.

(53) Berr, S. S.; Jones, R. R. M. *Langmuir* **1988**, *4*, 1247.

(54) Shanks, P. C.; Franses, E. I. *J. Phys. Chem.*, **1992**, *96*, 1794.

(55) Lu, J. R.; Marrocco, A.; Su, T. J.; Thomas, R. K.; Penfold, J. *J. Colloid Interface Sci.*, **1993**, *158*, 303.

(56) Quina, F. H.; Nassar, P. M.; Bonilha, P. M.; Bales, B. L. *J. Phys. Chem.*, **1995**, *99*, 17028.

(57) Bales, B. L.; Almgren, M. *J. Phys. Chem.*, **1995**, *99*, 15153.

(58) Chatterjee, A.; Moulik, S. P.; Sanyal, S. K.; Mishra, B. K.; Puri, P. M. *J. Phys. Chem. B*, **2001**, *105*, 12823.

(59) Bales, B. L. *J. Phys. Chem. B*, **2001**, *105*, 6798.

(60) Aswal, V. K.; Goyal, P. S. *Phys. Rev. E*, **2003**, *67*, 051401.

(61) Ropers, M. H.; Czichocki, G.; Brezesinski, G. *J. Phys. Chem. B*, **2003**, *107*, 5281.

(62) Vautier-Giongo, C.; Bales, B. L. *J. Phys. Chem. B*, **2003**, *107*, 5398.

(63) Bastiat, G.; Grassl, B.; Khoukh, A.; Francois, J. *Langmuir*, **2004**, *20*, 5759.

(64) Zana, R. *Dynamics of Surfactant Self-Assemblies: Micelles, Microemulsions, Vesicles, and Lyotropic Phases*; CRC Press: Boca Raton, FL 2005; Surfactant Science Series Vol. 125.

(65) Berendsen, H. J. C.; van der Spoel, D.; van Drunen, R. *Comp. Phys. Comm.* **1995**, *91*, 43.

(66) Lindahl, E.; Hess, B.; van der Spoel, D. *J. Mol. Model.* **2001**, *7*, 306.

(67) van der Spoel, D.; Lindahl, E.; Hess, B.; Groenhof, G.; Mark, A. E.; Berendsen, H. J. C. *J. Comp. Chem.* **2005**, *26*, 1701.

(68) Berendsen, H. J. C.; Postma, J. P. M.; van Gunsteren, W. F.; Di Nola, A.; Haak, J. R. *J. Chem. Phys.* **1984**, *81*, 3684.

(69) Miyamoto, S.; Kollman, P.A. *J. Comp. Chem.* **1992**, *13*, 952.

(70) Siepmann, J. I., Frenkel, D. *Mol. Phys.* **1992**, *75*, 59.

(71) Ferrenberg, A. M.; Swendsen, R. H. *Phys. Rev. Lett.*, **1988**, *61*, 2635.

(72) Panagiotopoulos, A. Z. *J. Phys.: Condens. Matter* **2000**, *12*, R25.

(73) Wilding, N. B. *Am. J. Phys.* **2001**, *69*, 1147.

(74) Weeks, J. D.; Chandler, D.; Andersen, H. C. *J. Chem. Phys.* **1971**, *54*, 5237.

(75) Pettit, B. M.; Rossky, P. J. *J. Chem. Phys.* **1986**, *84*, 5836.

(76) Koneshan, S.; Rasaiah, J. C. *J. Chem. Phys.* **2000**, *113*, 8125.

(77) Koneshan, S.; Rasaiah, J. C.; Lynden-Bell, R. M.; Lee, S. H. *J. Phys. Chem. B* **1998**, *102*, 4193.

(78) Åqvist, J. *J. Phys. Chem.*, **1990**, *94*, 8021.

(79) Stiles, P. J.; Hubbard, J. B.; Kayser, R. F. *J. Chem. Phys.* **1982**, *77*, 6189.

(80) Dang, L. X. *J. Am. Chem. Soc.* **1995**, *117*, 6954.

(81) Chandrasekhar, D.; Spellmeyer, D.; Jorgensen, W. L. *J. Am. Chem. Soc.* **1984**, *106*, 903.

(82) Martin, M. G.; Siepmann, J. I. *J. Phys. Chem. B* **1998**, *102*, 2569.

(83) Atkins, P. W. *Physical Chemistry*, Oxford University Press: Oxford, UK, 6th ed. 2001.

(84) Chandler, D. *Nature* **2005**, *437*, 640.

(85) Missel, P. J.; Mazer, N. A.; Carey, M. C.; Benedek, G. B. *J. Phys. Chem.* **1989**, *93*, 8354.

(86) see e.g. Baumgärtner, A. *J. Chem. Phys.* **1980**, *72*, 871. Micka, U.; Holm, C.; Kremer, K. *Langmuir* **1999**, *15*, 4033.

(87) Lazaridis, T.; Karplus, M. *Proteins* **1999**, *35*, 133.

(88) Bales, B. L.; Shahin, A.; Lindblad, C.; Almgren, M. *J. Phys. Chem. B*, **2000**, *104*, 256.

(89) Hoyer, H. W.; Marmo, A. *J. Phys. Chem* **1961**, *65*, 1807.

(90) Mehta, S. K.; Bhasin, K. K.; Kumar, A.; Dham, S. *Colloids and Surfaces A: Physicochem. Eng. Aspects* **2006**, *278*, 17.

(91) Bales, B. L.; Zana, R. *J. Phys. Chem. B*, **2002**, *106*, 1926.

(92) Oh, S. G.; Shah, D. O. *J. Phys. Chem* **1993**, *97*, 284.

(93) Jorgensen, W. L.; Gao, J. *J. Phys. Chem.*, **1986**, *90*, 2174.

(94) Bhatt, D.; Chee, R.; Newman, J.; Radke, C. J. *Curr. Opin. Colloid Interface Sci.* **2004**, *9*, 145.

(95) Ranganathan, R.; Tran, L.; Bales, B. L. *J. Phys. Chem. B*, **2000**, *104*, 2260.

(96) Adamson, A. W. *Physical Chemistry of Surfaces*, Wiley, New York, 4th ed. 1982.

(97) Nishikido, N. *J. Colloid Interface Sci.*, **1983**, *92*, 588.

(98) Ogino, K.; Kakihara, T.; Abe M. *Colloid Polym. Sci.*, **1987**, *265*, 604.